Electronic Supplementary Material (ESI) for Analyst.
This journal is © The Royal Society of Chemistry 2020

Electronic Supporting Information

The Dynamic Single-Cell Intracellular pH Sensing by a SERS-Active Nanopipette

Jing Guo[1], Alberto Sesena Ribfiaro[1], Yanhao Lai[2], Joseph Moscoso[1], Feng Chen[1,3], Yuan Liu[2], Xuewen Wang[1], Jin He[1]

[1]Department of Physics, Biomolecular Science Institute, Florida International University, 11200 SW 8th St., Miami, FL 33199, USA

[2]Department of Chemistry and Biochemistry, Biomolecular Science Institute, Florida International University, 11200 SW 8th St., Miami, FL 33199, USA

[3]School of biomedical engineering and informatics, Nanjing Medical University, Nanjing 211166, People's Republic of China

E-mail: jinhe@fiu.edu

Table of Contents

S1. Spring constant characterization of the nanopipette

The optical images of long-taper and short-taper nanopipette are shown in Figure S1A. We can see the short-taper is about half the length of long-taper. Figure S1B and C show the SEM images of side-view of long-taper and short-taper nanopipette, which can provide dimension information. From classical beam theory, the spring constant k for a hollow cylindrical tube can be approximated by Equation (1)[1] with the cantilever approximation.

$$k = \frac{3 * E * I}{L^3} \qquad (1)$$

Here $I \approx \pi * R^3 * t$ is the geometric moment of inertia of a cylindrical tube. E is the Young's modulus of the material (70 x10^9 N/m^2 for quartz). L is the length of the cylindrical tube. The model is shown in Figure S1D.

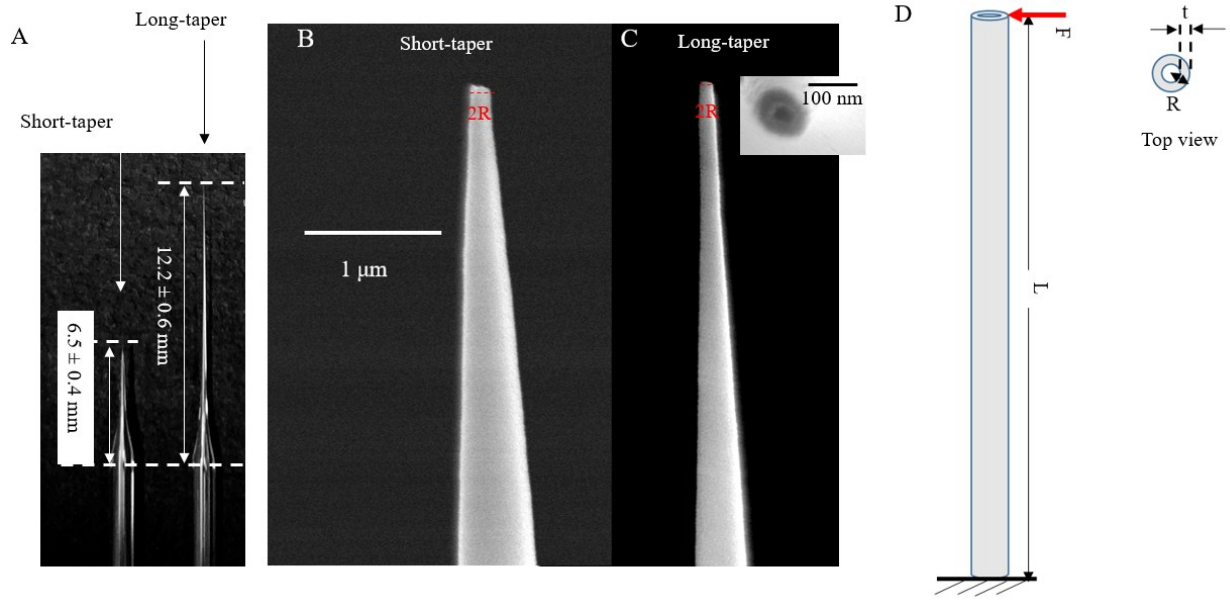

Figure S1. (A) Optical images of short-taper and long-taper nanopipettes. (B) and (C) SEM images of short-taper and long-taper nanopipette, respectively. The inset image in (C) is the top view of long-taper nanopipette. (D) Schematic drawing of the cantilever approximation model for the beam theory.

Here, we treated the tip section as a cylindrical tube with the radius R. The radius is indicated in the Figure S1B and C with red line. The thickness t of the tube can be estimated from the top view of nanopipette as indicated in the inset of Figure S1C. The derived spring constant k is around 0.056 N/m and 0.504 N/m for long-taper and short-taper nanopipette by using Equation 1, respectively.

S2. The assignment of SERS bands for 4-MBA molecule

We have used density functional theory (DFT) (Gasussian 09 package) to calculate the Raman spectra of 4-MBA molecule on gold. The geometry of the Au3-4-MBA molecular model with neutral charge is shown in Figure S2A. The gold NP was represented by a Au3 cluster. The DFT calculation was conducted based on the energy minimized ground-state geometry using hybrid exchange–correlation functional (B3LYP). The 6-31G** basis set was used for molecule and LANL2DZ basis set was used for gold atoms. As shown in Figure S2 B, the calculated and measured SERS spectra of 4-MBA (at pH 4.2)

matched very well. The mode assignments to the SERS spectrum based on the DFT calculation are summarized in the table of Figure S2C.

A

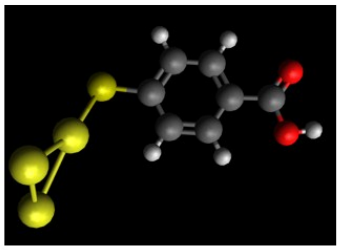

B

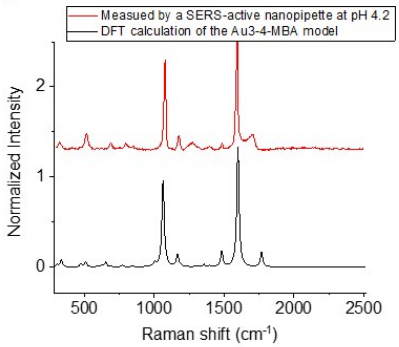

C

4-MBA	
Assignment	**Raman shift (cm^{-1})**
ν(CS) (b2)	320
γ(CCC) (ring, out-of-plane bending)	516
δ(COOH) (in-plane-bending)	688
δ(COO^-) (in-plane-bending)	847
Ring breathing (a1)	1012
ν(CC)+ν(CS) (a1)	1077
δ(CH) (in-plane-bending (a1))	1186
ν(COO^-)(stretching)	1400
ν(CCC) (Ring stretch (a1))	1592
νC=O (stretching)	1703

Symbols: *ν*, stretching; *δ*, deformation or in-plane bending; *γ*, π, out-of-plane bending; *ω*, wagging; *τ*, torsion; *ρ*, rocking; s, symmetric; as, antisymmetric.

Figure S2. (A) Molecular structure of the Au3-4-MBA model used for the DFT calculation. (B) The SERS spectrum measured from a SERS-active nanopipette tip at the acid condition (red color) and the DFT calculated Raman spectrum (black color). (C) The table of Raman bands assignment for 4-MBA.

S3. The difference between calibration and live-cell experiments.

Figure S3 shows the schematic of the experimental setup for the calibration (Left) and the actual (Right) live-cell experiments. The main difference is that the nanopipette tip position is different. The nanopipette tip needs to be very close to the cover glass surface to get into the cell for the intracellular sensing. Thus, the cover glass is close to the focus plane of the lens. Therefore, we observed the weak Raman signal from the cover glass in the intracellular measurement, as shown in the spectra of Figure S3C. In the calibration, no Raman signal was observed from the cover glass. In addition, the Raman signal of live-cell experiment is generally weaker, likely due to the extra light scattering by the cell. We therefore used a longer exposure time of 2 s for the live-cell experiment. Although the signal-to-noise ratio is obviously increased, the tradeoff is that the water peak becomes noticeable with the longer exposure time. Fortunately, there is still a clean spectral window in the Raman spectra for the pH sensing, as highlighted with the green color in the spectra of Figure S3C. This is the other reason I_{1400}/I_{1077} was used as the pH probe.

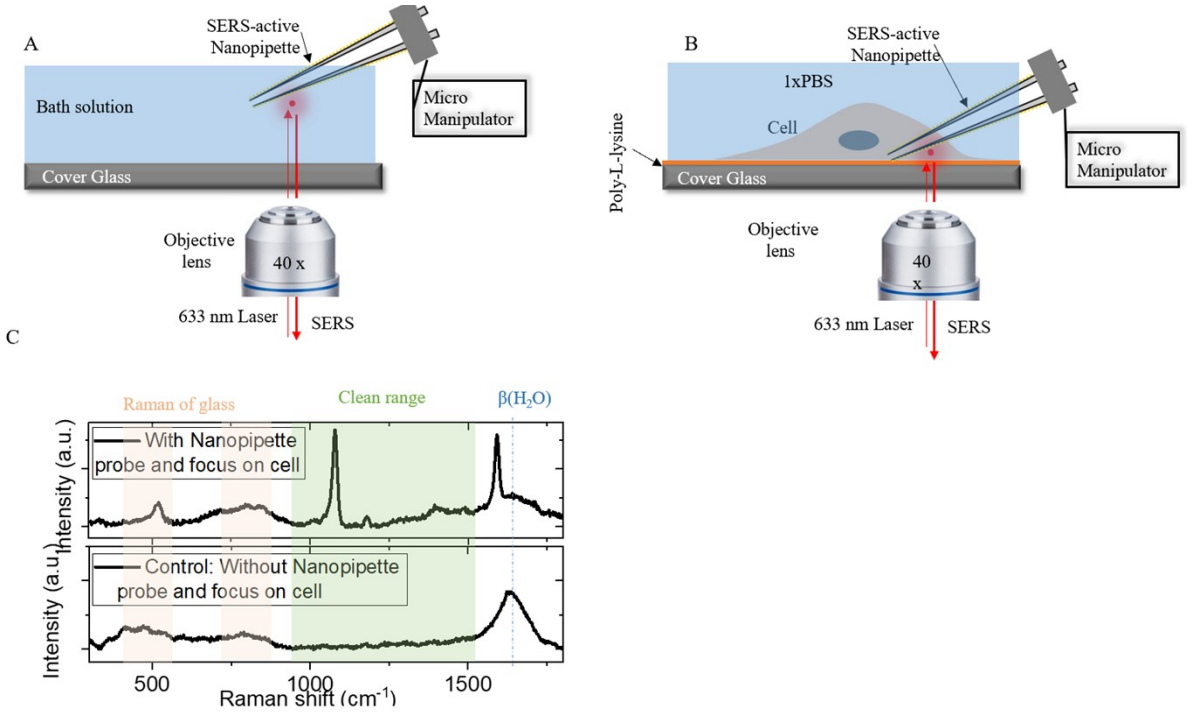

Figure S3. (A-B) Schematic of the experimental setup for the calibration (A) and actual intracellular sensing (B) experiments using the pH-sensitive nanopipette. (C) Top: Typical SERS spectrum acquired by a pH-sensitive nanopipette tip inside a cell. Bottom: Typical Raman spectrum of the cover glass with the absence of a SERS-active nanopipette, the exposure time is 2 s per frame.

S4. Time-resolved SERS spectra taken by a nanopipette loaded with basic solution inside the nanopore barrel at zero bias

In the main text, we have showed that the basic solution loaded in the nanopore barrel can be released electrically by an applied bias and locally change the pH near the apex of the nanopipette. This process is well-controlled by the applied bias in the nanopore barrel. At zero bias, no observable spectral changes were observed. One typical time-resolved SERS trajectory at zero bias is shown in Figure S4.

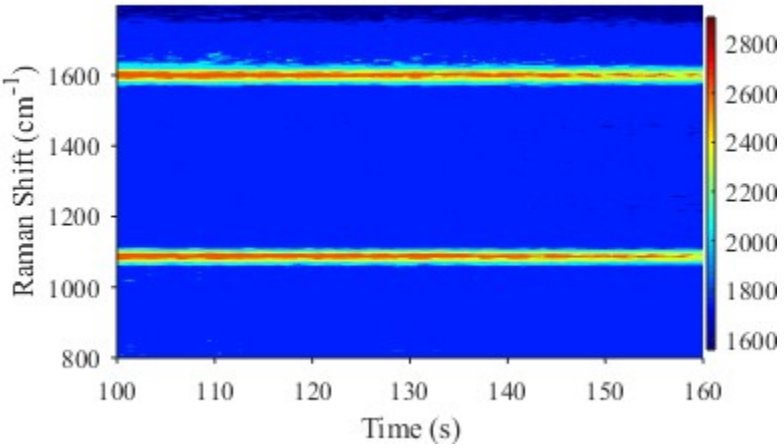

Figure S4: Heatmap of time-resolved SERS spectra (1 s per frame) at zero bias.

S5. Optical microscope images for the pH sensing of Fibroblast cells with a nanopipette probe.

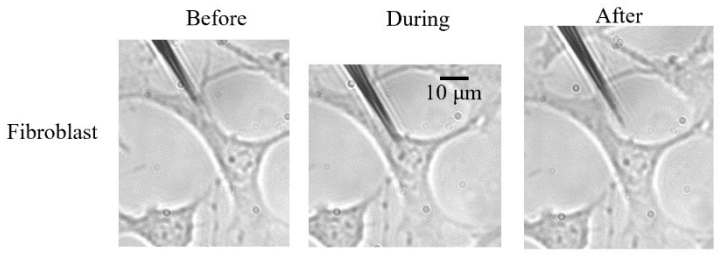

Figure S5. Bright-field microscope images of Fibroblast cells before, during and after the insertion of a SERS-active nanopipette tip.

S6. Cell damage test

We used a Trypan blue assay to evaluate the cellular damage induced by the intrusion of the long-taper nanopieptte. A stiff nanopipette was used as the control. Fibroblast live cells on the cover glass are immersed in 1xPBS with 0.04% Trypan blue dye. When observed by naked eyes using the microscope, the cell inserted by the short-taper nanopipette tip shows blue color only after 2 mins, suggesting the cell is dying. Recorded by a black and white CCD camera, the dead cell appears darker (enclosed by the blue color circle) in the gray-scale image, as shown in the left panel of Figure S6. However, the cell inserted by the long-taper nanopipette tip still remains clear in the image after 60 mins, as shown in the right panel of Figure S6.

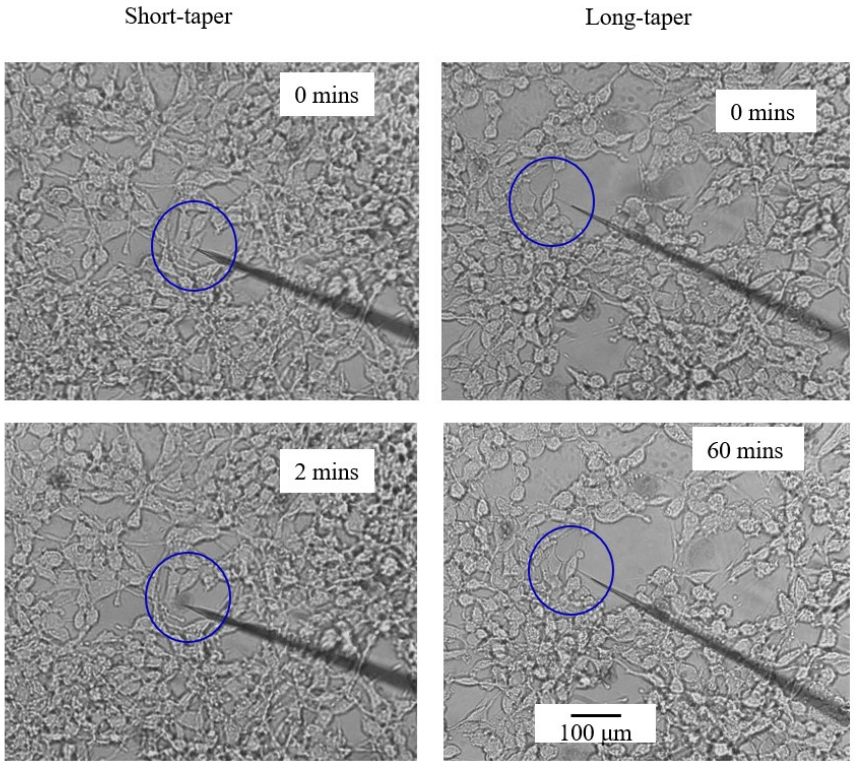

Figure S6. Optical images of Fibroblast cells immersed in 1xPBS buffer solution with 0.04% trypan blue. Left: Insertion of a short-taper nanopipette probe. Right: Insertion of a long-taper nanopipette probe.

S7. pH_i of Fibroblast and Hela cells in pH_e=7.4 buffer

The pH_i values of Fibroblast and Hela cells in 1xPBS (pH_e = 7.4) were measured. Figure S7 shows the measured pH_i under the neutral environment.

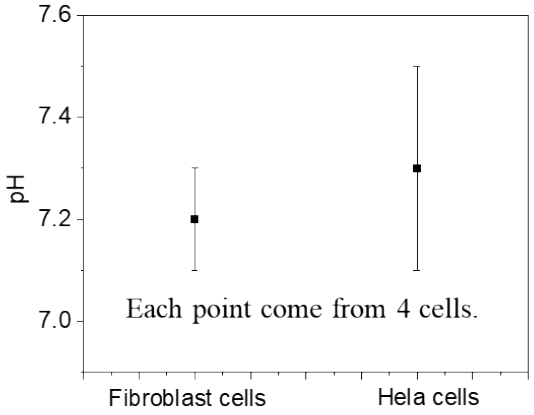

Figure S7. The mean pH_i of Fibroblast and Hela cells are the average values obtained from 4 cells in 1xPBS solution (pH_e = 7.4).

S8. The calibration curve for Nanopipette probe

Figure S8A shows the SERS response of nanoprobe1 to different bath solution pH before (Pre-calibration) and after (Post-calibration) the live-cell intracellular pH sensing exeriments. Figure S8B(i) shows the I_{1400}/I_{1077} at different pH. The SERS changes of pre-calibration and post-calibration are not exactly overlapped. Therefore, the average curve of pre- and post-calibration curves was used for the intracellular pH determination. Using same method, calibration curve of nanoprobe2 was obtained, as shown in Figure S8B(ii).

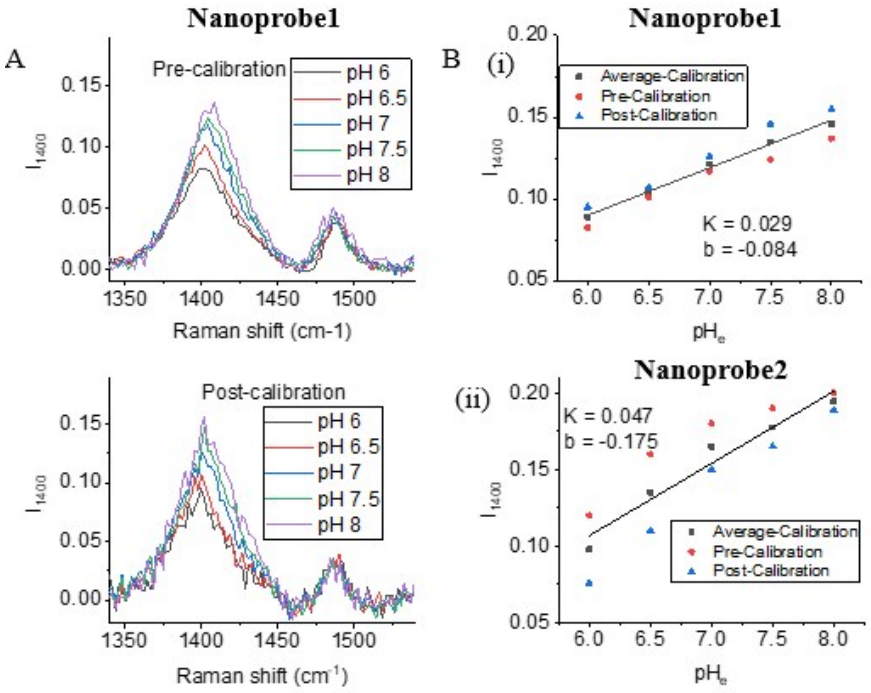

Figure S8. (A) SERS spectra of the nanoprobe1 in phosphate buffer solutions with differnet pH before (top) and after (bottom) the intracellular pH sensing experiments. (B)((i)-(ii)) The linear calibration curves of Nanoprobe1 ((i), $R^2 = 0.99$) and nanoprobe2 ((ii), $R^2 = 0.97$) used for pH_i sensing.

S9. Recipe for the preparation of phosphate buffer with different pH

The concentrations of salt components in the phosphate buffer solution are: $C_{(KCl)}$ = 2.7 mM; $C_{(NaCl)}$ = 137 mM; $C_{(K_2HPO_4)}$ +$C_{(KH_2PO_4)}$ = 10 mM. To prepare the phosphate buffer at different pH, the $C_{(K_2HPO_4)}$ and $C_{(KH_2PO_4)}$ are adjusted individually while keeping their sum concentrations always at 10 mM. The detailed changes in the salt concentration are shown in table S1 below.

Final phosphate buffer component concentration				
pH	$C_{(K2HPO4)}$ (mM)	$C_{(KH2PO4)}$ (mM)	$C_{(KCl)}$ (mM)	C(NaCl) (mM)
6.0	1.00	9.00	2.7	137
6.5	1.88	8.12	2.7	137
7.0	3.02	6.98	2.7	137
7.5	3.63	6.37	2.7	137
8.0	3.87	6.13	2.7	137

Table of S1. The component concentration list of phosphate buffer with different pH.

Reference

1. Jayant, K., et al., *Flexible Nanopipettes for Minimally Invasive Intracellular Electrophysiology In Vivo.* Cell Reports, 2019. **26**(1): p. 266-278.e5.